

A Landing Buffer System for Vertical Takeoff and Vertical Landing Reusable Launch Vehicle

Wang Dongliang*, Cui Qifeng, Luohaijun, Li Ming
Aerospace System Engineering Shanghai, Shanghai 201109, P.R.China
wangdongliang@asesspace.com

Abstract

Guided by the research and application of vertical takeoff and vertical landing reusable launch vehicles (VTVL RLV) by SpaceX and Blue Origin, reuse has gradually become a major development trend of launch vehicles in recent years. For the RLV, the landing buffer system is a necessary constitution for the landing procedure.

Compared with other mature launch vehicle technologies, landing buffer system is a new field, which involved many key technologies, such as lightweight structure, reliable hold-down and release mechanism, deployment and locking mechanism, energy absorption, stability optimization, thermal insulation, and etc. A large number of investigation and verification are required for each, or combined key technologies, which indicates the complexity and difficulties of the landing buffer system during the development.

In this paper, a VTVL RLV landing buffer system is proposed. The general design and principle of the system are elaborated, and the relevant key components are demonstrated. The dynamics and kinematics of the landing buffer system are analyzed. The landing stability under complex conditions is simulated and analyzed, which verifies the feasibility of the landing buffer system.

Keyword: VTVL; RLV; Landing buffer system

1.Introduction

In recent years, with the successful commercial use by SpaceX and Blue Origin, vertical landing reusable launch vehicles (VTVL RLVs) have received widely attention. VTVL RLVs are capable of carrying payload into orbit and then taking valuable parts of the vehicle back to earth for next flight so that reduce the lunch cost significantly [1]. Of all the recovery steps, landing is one of the most crucial because a slight malfunction could result in failure of the reuse. Some corporations before SpaceX and Blue Origin have designed and tested the VTVL RLVs with landing buffer systems in several projects. The landing buffer system can be mainly grouped into several categories, retro-rocket, parachute deceleration device, cushion airbag, landing legs mechanism, and etc [2]. Both the Viking and Phoenix Mars Rovers landed successfully through parachute deceleration [3]; The retro-rocket ignites before touching the ground, and the vehicle receives the reverse thrust, which generates upward acceleration and makes the vehicle decelerate [4]. The airbag landing has large contact area, so the impact acceleration is small and the cushioning effect is good. However, it is susceptible to the influence of external environment, poor stability and easy to rebound, jump or even roll. The landing leg mechanism enabled the "Surveyor" lunar probe and the Apollo manned lunar module to achieve a successful soft landing which use honeycomb buffer without reusable function [5]. Considering the uncertainties of initial landing conditions and reusability of the vehicle, it becomes crucial to design a reusable landing buffer system that can improve landing stability as well as reduce landing impact overloads.

Based on the above motivations, this paper proposes a reusable landing buffer system configuration for a VTVL RLV to address different initial landing conditions. Mathematical modeling and calculation of the proposed landing buffer system is established and landing stability analysis is performed.

2.Overall Scheme

The landing buffer system has 4 same landing legs, each leg consists a main strut, two tandem buffers, a shell, a pusher, a set of hold-down and release mechanism (HDRM) and 3 joints. The overall scheme of the landing buffer system is shown in Fig. 1.

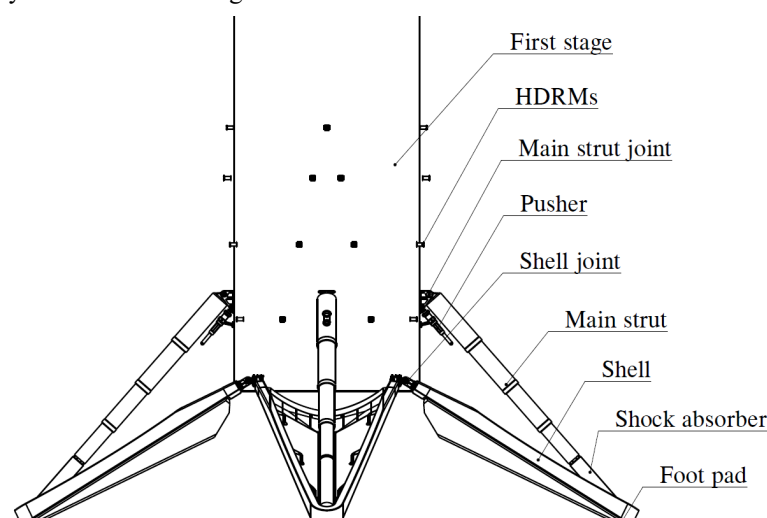


Figure.1 Overall scheme

The working principle of the landing buffer system is as follows:

- a. The landing buffer system is stowed on the rocket body by the HDRMs [6] which bear the

vibration environment. The whole landing buffer system is wrapped on the surface of the rocket body by the aerodynamic designed shell to reduce the aerodynamic force and heat.

- b. Before the rocket touchdown, the HDRMs unlock and release the main strut and the shell. The entire landing buffer system will cross the “Dead point” by the pusher which drove by the compressed air.
- c. After the landing buffer system passes through the dead-point position, the main strut is deployed and locked with the inner cylinder latch [7][8], and the shell is driven to expand in place. The aerodynamic design of the shell during the deployment process minimizes the impact of the landing buffer system on the attitude of the rocket, and at the same time, to a certain extent, protects the landing buffer system from the exhaust flame ablation.
- d. When the rocket touchdown, the foot pad mounted on the shell touches the ground, and the buffer (shock absorber) mounted on the main strut absorbs the landing shock and energy, so as to achieve the purpose of cushioning, and finally achieve the soft landing of the rocket. The shock absorber consists of two parts, one of them is a reusable pneumatic-hydraulic buffer, and the other one is a honeycomb buffer which works as a safer to limit the load to the landing buffer system.

3. Mathematical Modeling and Engineering Calculation

In this section, the touchdown and shock absorbing process of the landing buffer system are mathematical modeled. With these models, engineering calculation can be conducted for the engineering design.

3.1 Kinematic Analysis

Kinematic Analysis of the landing and shock absorbing process is performed to one leg of the landing buffer system, and simplifications and assumptions are made as follows:

- a. At a certain time of the process, the rocket body moves at a vertical acceleration “ a ” and velocity “ V ”, without considering the translation and rotation of other degrees of freedom of the rocket body;
- b. The motion process is analyzed for only one landing leg, Point A is the foot pad and moves along horizontal direction, and Point B is the shell joint point and moves along the vertical direction, AB is the simplification of the shell.

The kinematic analysis sketches are as show in Figure.2.

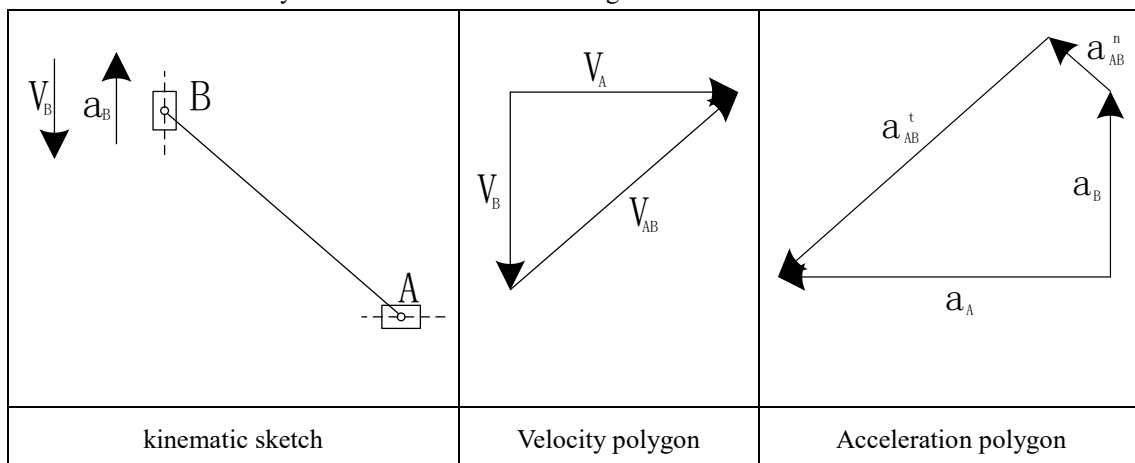


Figure.2 Kinematic Analysis

The velocity vector equation and the acceleration vector equation of the shell are as follows:

$$V_A = V_B + V_{AB} \quad (1)$$

$$a_A = a_B + a_{AB}^n + a_{AB}^r \quad (2)$$

Whereas

$$a_{AB}^n = \omega_{AB}^2 L_{AB} + a_{AB}^r \quad (3)$$

$$a_{AB}^r = \varepsilon_{AB} L_{AB} \quad (4)$$

3.2 Dynamic Analysis

Dynamic Analysis is performed to the foot pad and the shock absorber, the local wind impact on the rocket body is not considered.

For the foot pad, the force analysis is show in Figure.3.

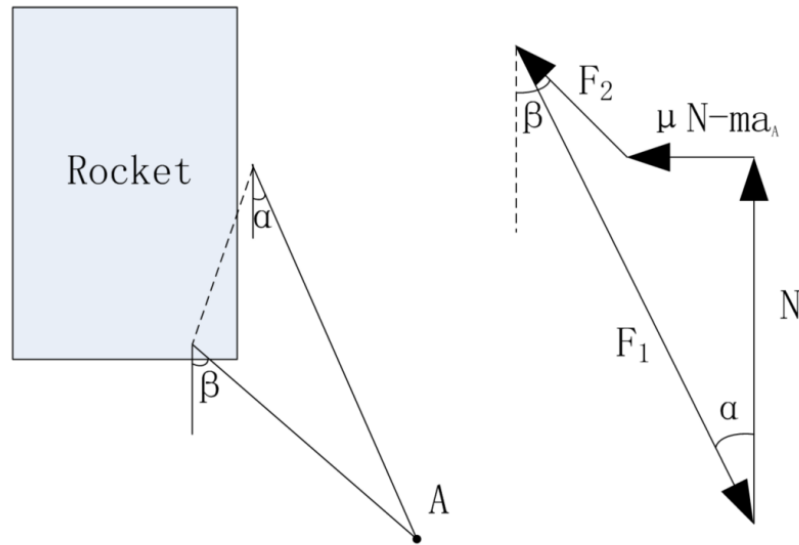


Figure.3 Force analysis of the foot pad

Whereas:

F_1 —Axial load of the main strut;

F_2 —Axial load of the shell;

N —Load on foot pad from ground;

α —Angle between the main strut and the gravity vector;

β —Angle between the shell and the gravity vector;

m —Mass of the foot pad;

μ —Footpad/soil friction coefficient;

$-ma_A$ —Inertia force of the foot pad.

For the shock absorber, the axis force of the honeycomb buffer can be simplified as a constant value while the force of pneumatic-hydraulic can be described as below [9]:

$$f = f_h + f_a + f_f + f_s \quad (5)$$

$$f_s = \begin{cases} K_S S & S < S_0 \\ 0 & S_0 \leq S \leq S_{\max} \\ K_S (S - S_{\max}) & S > S_{\max} \end{cases} \quad (6)$$

$$f_a = A_a \left[p_0 \left(\frac{V_0}{V_0 - A_a S} \right)^N - p_{atm} \right] \quad (7)$$

$$f_h = \begin{cases} \frac{\rho(A_h + A_+) A_h^2 \dot{S}^2}{2C_d A_+^2} & (\dot{S} \geq 0) \\ -\frac{\rho(A_h + A_-) A_h^2 \dot{S}^2}{2C_d A_-^2} & (\dot{S} < 0) \end{cases} \quad (8)$$

$$f_f = \mu_m f_a \frac{\dot{S}}{|\dot{S}|} \quad (9)$$

Whereas:

f_s —absorber structure limited force;

f_a —air chamber force;

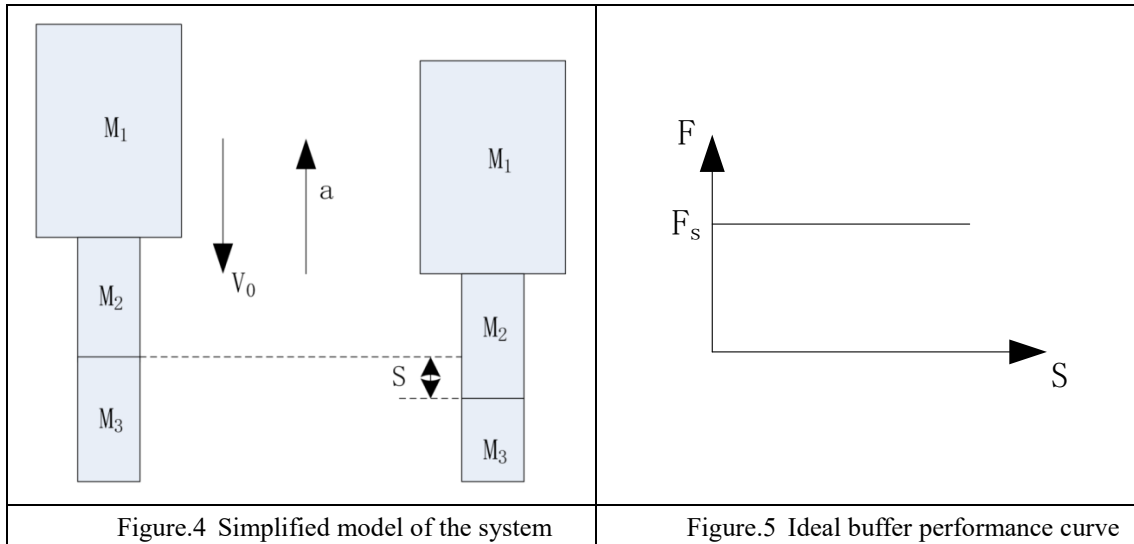
f_h —hydraulic damping force;

f_f —structure friction force.

3.3 Energy Analysis

The assumptions for the energy analysis are made as follows:

- M_1 、 M_2 are the simplification of the rocket and the main strut, and they are connected to each other as M_{1+2} ;
- The shock absorber is assumed an ideal buffer with 100% efficiency which with the performance curve as Figure.5, and the performance of the buffer is not related to the landing speed, the real performance of the buffer can be calculated by efficiency coefficient “ η ”. The mass of the buffer is M_3 ;
- The entire system touchdown with initial velocity “ V_0 ”, the buffer works with the load “ F_s ” and make the system accelerate a uniformly decelerating motion to a stationary state as “ a ”, the total length of the shock absorbing process is “ S ”;
- All the energy of the rocket from initial speed to stationary state are totally absorbed by the buffer system and no kick-back occurred.



Based on the above simplification and assumption, according to the conservation of energy, the equation of the system can be described as:

$$F_S \cdot S \cdot \eta = \frac{1}{2} M_{1+2} V_0^2 + M_{1+2} \cdot g \cdot S \quad (10)$$

For the main strut and the rocket, there is:

$$F_S - M_{1+2} \cdot g = M_{1+2} \cdot a \quad (11)$$

Where the rocket decelerating “a” of the system is limited by the structure ability of the rocket.

The equation of energy can be expressed as Figure.6 which including the information as follows:

- The range of F_s is between $M_{1+2} \cdot g$ and $M_{1+2} \cdot a$, the upper limit is determined by the rocket structure ability;
- The red area $M_{1+2} \cdot g \cdot S$ means the potential energy of the system is directly proportional to the total landing mass and the shock absorb length;
- The blue area $\frac{1}{2} M_{1+2} V_0^2$ means the kinetic energy can be considered as a constant value because the mass of rocket is much larger than the landing buffer system;
- The critical parameter for shock absorber F_s and S can be chosen on the line of dashes and they are the input of the shock absorber design.

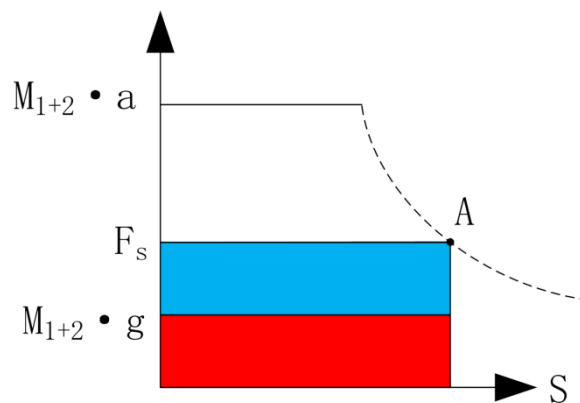


Figure.6 Energy sketch map of the system

4. Stability Simulation Analysis

To verify the above calculation, a virtual prototype of the landing buffer system has been established, the stability simulation has performed and the adaptability of landing conditions is analyzed. In this paper, landing conditions are divided into two categories to reduce the amount of the simulation computing and identify the sensitive factors of safety landing more efficiently. One of them is the altitude landing conditions and the other one is landing sit local conditions, both of them consists of various landing parameters. The simulation performed with these parameters separately first and then combined together.

4.1 Altitude landing conditions Analysis

Attitude landing conditions mainly include the deviation angle between the X-axis of the rocket and the local gravity vector, the angular velocity and linear velocity in three directions of the rocket body which are all controlled by the rocket engine. Because the deviation angle at the touchdown moment has a great influence on the landing performance, the landing conditions under different deviation angles which named as different cases [10][11] in Figure.7 are analyzed first to find out the worst conditions in each landing case.

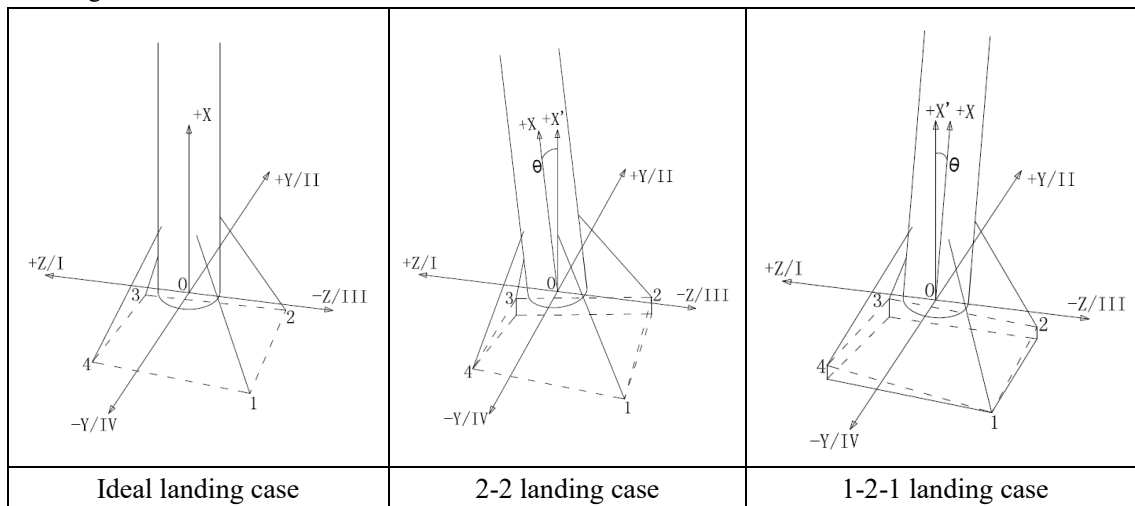


Figure.7 Landing case

In the figure above, OXYZ is the body coordinate of the rocket, X axis is along the rocket body axis; $+X'$ is the local gravity vector; 1~4 are the identify number of the landing legs. To focus on the effective simulation results and find the worst landing conditions more efficiently, leg 1 is defined as the evaluation object when simulation results checking and the maximum values of the landing control ability are applied as the simulation input which shown in Table.1.

Table.1 Landing conditions of altitude control

Landing conditions No.	Θ	ω_x	ω_y	ω_z	V_x	V_y	V_z	comments
	°	°/s	°/s	°/s	m/s	m/s	m/s	
C1.	0	0	2	-2	-3.71	0.7	0.7	
C2.	0	0	2	-2	-3.71	-0.7	-0.7	Ideal landing case;
C3.	0	1.5	2	-2	-3.71	0.7	0.7	4 legs touchdown together
C4.	0	1.5	2	-2	-3.71	-0.7	-0.7	
C5.	5	0	2	-2	-3.71	0.7	0.7	2-2 landing case;
C6.	5	0	2	-2	-3.71	-0.7	-0.7	Leg 1 and leg 2 touchdown together first
C7.	5	1.5	2	-2	-3.71	0.7	0.7	and then the other 2 followed together

Landing conditions No.	Θ °	ω_x °/s	ω_y °/s	ω_z °/s	Vx m/s	Vy m/s	Vz m/s	comments
C8.	5	1.5	2	-2	-3.71	-0.7	-0.7	
C9.	5	0	2	-2	-3.71	0.7	0.7	1-2-1 landing case; leg 1 touchdown first followed by leg 2 and 4 together and then the leg 3 ended
C10.	5	0	2	-2	-3.71	-0.7	-0.7	
C11.	5	1.5	2	-2	-3.71	0.7	0.7	
C12.	5	1.5	2	-2	-3.71	-0.7	-0.7	

Whereas:

Θ —Angle between the X-axis of the rocket body and the local gravity vector

ω_x —Roll angular rate

ω_y —Yaw angular rate

ω_z —Pitch angular rate

Vx—Vertical velocity

Vy—Horizontal velocity in Y-direction

Vz—Horizontal velocity in Z-direction

The simulation results are shown in Table.2, footpad/soil friction coefficient is 0.4 and local wind force is not considered.

Table.2 Landing conditions simulation results

Landing conditions No.	Overload of C.G. g	Maximum load of the main strut N	Maximum load of the shell N	comments
C1.	2.52	3.76E+05	1.65E+05	
C2.	2.32	4.19E+05	1.14E+05	Ideal landing case
C3.	2.52	3.69E+05	1.66E+05	
C4.	2.32	4.19E+05	1.17E+05	
C5.	1.36	4.15E+05	1.85E+05	
C6.	1.36	5.33E+05	2.77E+05	2-2 landing case
C7.	1.30	4.16E+05	1.85E+05	
C8.	1.35	5.36E+05	2.77E+05	
C9.	1.57	4.56E+05	1.85E+05	
C10.	1.66	9.43E+05	3.73E+05	1-2-1 landing case
C11.	1.57	4.55E+05	1.86E+05	
C12.	1.64	9.44E+05	3.74E+05	

The calculated results shown that the landing loads on the main trust and shell are not sensitive to the roll angular rate but both of them reach the maximum value when the linear velocity combined with the yaw and pitch angular rate toward the same single leg from the rocket body.

4.2 Local landing Conditions

3 calculated maximum load of the main strut cases in Table.2 are chosen as the worst conditions for coupling with the local landing conditions which mainly includes the local wind force and footpad/soil friction coefficient. The landing conditions are shown in Table.3.

Table.3 Local conditions coupled with worst altitude conditions

Landing conditions	Θ	ω_x	ω_y	ω_z	Vx	Vy	Vz	Fw	μ
No.	°	°/s	°/s	°/s	m/s	m/s	m/s	N	/
C13.									0.2
C14.								4722	0.4
C15.									0.6
C16.									0.8
C17.				C4					0.2
C18.								-4722	0.4
C19.									0.6
C20.									0.8
C21.									0.2
C22.								4722	0.4
C23.									0.6
C24.									0.8
C25.				C8					0.2
C26.								-4722	0.4
C27.									0.6
C28.									0.8
C29.									0.2
C30.								4722	0.4
C31.									0.6
C32.									0.8
C33.				C12					0.2
C34.								-4722	0.4
C35.									0.6
C36.									0.8

Whereas:

Fw——calculated local wind force, direction point to the leg 1.

μ ——footpad/soil friction coefficient

The simulation results of the above conditions are shown in Table.4 which shown that the conditions of 1-2-1 landing case result in significant large load on the main strut and the shell and the honeycomb buffer activated.

Table.4 coupled conditions simulation results

Landing conditions	Overload of	Maximum load of the main	Maximum load of the
No.	C.G.	strut	shell
	g	N	N
C17.	1.95	4.27E+05	1.22E+05
C18.	2.39	4.23E+05	1.05E+05
C19.	2.98	4.19E+05	0.91E+05
C20.	3.83	4.11E+05	0.91E+05
C21.	1.17	6.25E+05	2.91E+05
C22.	1.36	5.60E+05	2.77E+05

Landing conditions No.	Overload of	Maximum load of the main	Maximum load of the
	C.G.	strut	shell
	g	N	N
C23.	1.87	5.22E+05	2.81E+05
C24.	2.69	5.03E+05	2.86E+05
C25.	1.13	5.68E+05	2.76E+05
C26.	1.36	5.08E+05	2.70E+05
C27.	1.87	4.67E+05	2.65E+05
C28.	2.69	4.41E+05	2.63E+05
C29.	1.77	9.89E+05	3.83E+05
C30.	1.68	9.84E+05	3.89E+05
C31.	1.55	9.12E+05	3.69E+05
C32.	1.34	8.03E+05	3.38E+05
C33.	1.61	9.07E+05	3.57E+05
C34.	1.62	9.06E+05	3.57E+05
C35.	1.57	8.35E+05	3.39E+05
C36.	1.36	7.32E+05	3.13E+05

5. Conclusions

- (1) A landing buffer system configuration for a VTVL RLV is proposed; the overall scheme and the working principle are demonstrated.
- (2) Kinematics equations, Dynamic equations and energy equations are established for the system, a virtual prototype of the landing buffer system has been established for verifying the designed system.
- (3) Altitude and local landing conditions are considered separately and then combined for the different landing cases simulation, the calculated results shown that the landing loads on the main trust and shell are not sensitive to the roll angular rate but both of them reach the maximum value when the linear velocity combined with the yaw and pitch angular rate toward the same single leg from the rocket body. When local wind force on the landing site applied, loads on the trust and the shell will rise significantly, and the 1-2-1 landing case will activate the honeycomb shock absorber.

References

- [1] Z.H.Pan. 2016. Significance and Key Technologies of Recovery Rocket. *Science & Technology Review*. 01:15-19.
- [2] Robert D.Braun, Robert M Manning. 2007. Mars Exploration Entry, Descent, and Landing Challenges. *Journal Of Spacecraft And Rockets*. 44:310-323.
- [3] Y.B.Hu, Y.Sun. 2010. Soft Lander of Lunar Lander. *Aerospace Shanghai*. 01:43-50.
- [4] B.H.Lin. 1996. Overview of Landing Buffer Technology. *Spacecraft Recovery & Remote Sensing | Spacecraft Recov Remot Sens*. 03:1-16.
- [5] X.Y.Liu. 2013. Stability simulation analysis of soft landing buffer for Lander. PhD Thesis. Hunan University.
- [6] Q.Shen. 2016. Performance Analysis of A Typical Landing Gear Uplock Device. *Equipment Manufacturing Technology*. 05:82-85.
- [7] W.W.Ao, H.P.Pei, H.Chen. 2012. Study of Landing Gear Actuating Cylinder's Inner-lock. *Mechanical Science and Technology for Aerospace Engineering*. 31: 130-134.
- [8] Y.Hou, M.Zhan, Q.B.Yuan, Z.G.Li, R.Xu, C.C.Kang, J.Xiao. 2016. Research on the parameters design of inner lock for the aircraft landing gear retract actuator. *Machine Design and Manufacturing Engineering*. 45: 74-78.
- [9] Y.X.Luo. 2015. The dynamic and static curve simulation of gas-hydraulic buffer. PhD Thesis. Northwestern Polytechnical University.
- [10] G.A. Zupp. 2013. An Analysis and a Historical Review of the Apollo Program Lunar Module Touchdown Dynamics, Technical Report NASA Johnson Space Center, Houston, TX.
- [11] J.Z. Ding, C.J. Wassng. 2016. Fast modeling for lunar lander dynamic analysis, AIAA Modeling and Simulation Technologies Conference, San Diego, California, USA.